South African Journal of Chemical Engineering 54 (2025) 357–370

Contents lists available at ScienceDirect

South African Journal of Chemical Engineering

journal homepage: www.elsevier.com/locate/sajce

Water hyacinth derived activated carbon electrode materials for water defluoridation using capacitive deionization technology

Hassan Johnson Kalilo [a], Joyce Elisadiki [b], Maheswara Rao Vegi [a,*], Said Ali Hamad Vuai [a]

[a] Department of Chemistry, College of Natural and Mathematical Sciences, The University of Dodoma, P.O. Box 338, Dodoma, Tanzania
[b] Department of Physics, College of Natural and Mathematical Sciences, The University of Dodoma, P.O. Box 338, Dodoma, Tanzania

ARTICLE INFO

Keywords:
Water hyacinths
Defluoridation
Activated carbon
Capacitive deionization (CDI)

ABSTRACT

Safe water is a vital component of human life that requires purification to reduce the concentration of ionic pollutants using appropriate water treatment techniques, such as capacitive deionization (CDI) water treatment technology. The porous activated carbon electrode materials have prepared via the carbonization of water hyacinth plants followed by chemical activation using KOH at different temperatures (400-700°C with an increment of 100°C) labeled as CWH-400, WHAC-500, WHAC-600 and WHAC-700 all being activated for 1 h where CWH represents carbonized water hyacinths and WHAC represents water hyacinths activated carbon. The activation temperature has a significant effect on the specific surface area of the porous carbon prepared, as it increases from 464.67 m^2/g for CWH-400 to 1020.01 m^2/g for WHAC-700. The defluoridation experiments were done using water samples with initial fluoride concentrations of 4.21, 4.61 and 3.51 mg/L for water samples from Arusha (A), Manyara (B) and Shinyanga (C) respectively when the 2 V was supplied to the cell with 10 mL/min flow rate at 3 hours charging time. The defluoridation results were 1.28, 1.37, and 1.15 mg/L for water samples A, B, and C, respectively. The WHAC-700 electrode was found to possess a capacitance of 501.89 F/g, exhibiting removal efficiencies of 69.60%, 70.28%, and 67.24% for water samples from Arusha (A), Manyara (B), and Shinyanga (C), respectively, at a potential of 2 V with a charging time of 3 hours. Therefore, the water hyacinth plants are suitable precursors for preparing porous activated carbon electrodes to be used in a CDI cell for the defluoridation of any water sample.

1. Introduction

Water is a vital component in the lives of humans and other living organisms. Human beings depend mainly on water to run several activities, such as domestic uses, agricultural, and industrial activities (Chowdhury, 2019; Lacson, 2021). It is estimated that 783 million people in the world lack safe drinking water due to pollution arising from fluoride (F^-) contamination, as well as mineral pollutants such as heavy metals (Lacson, 2021; Singh et al., 2017). Kumar et al. (2017) reported that fluoride contamination occurs naturally due to the variation in the chemical composition of the soil and rock structure in a particular area. Fluoride levels in sub-Saharan Africa have been reported to be high in Eastern Africa, especially along the Rift Valley. Tanzania was reported to have the highest levels of fluoride, followed by Kenya, Ethiopia, and Eritrea. In Tanzania, the fluoride distribution episode includes the Manyara region (46 mg/L), Arusha region (32 mg/L), Kilimanjaro (29 mg/L), Singida (21.3 mg/L), and Shinyanga (17 mg/L), in which the most affected areas are on the foothills of Mount Meru and Kilimanjaro (Kitalika et al., 2018; Mihayo et al., 2022).

A fluoride concentration below 1.5 mg/L plays a vital role in the health of human beings, particularly in bone formation (Saldaña-robles et al., 2023; WHO, 2003). The presence of high concentration of fluoride in drinking water can result into fluorosis effects in humans including dental, skeletal, and incapacitating (crippling) fluorosis (Biglari, 2016; Kim, 2011). The fluoride concentration ranging from 1.5 – 4.0 mg/L causes dental fluorosis, from 4.0 – 10 mg/L causes skeletal fluorosis and >10 mg/L causes crippling fluorosis (Ali et al., 2019; Lacson, 2021; Meenakshi, 2006; Mohapatra, 2009; WHO, 2011). Kabir (2020) reported that approximately 80 million people in East African Rift Valley countries are experiencing different fluorosis symptoms because they consume water contaminated with a high fluoride concentration above the WHO's permissible limit of 1.5 mg/L (WHO, 2019).

Several defluoridation methods have been developed to reduce the concentration to the recommended limits of 1.5 mg/L by the World

* Corresponding author.
E-mail addresses: vegimahesh@gmail.com, vegi.rao@udom.ac.tz (M.R. Vegi).

https://doi.org/10.1016/j.sajce.2025.08.013
Received 16 March 2025; Received in revised form 1 July 2025; Accepted 22 August 2025
Available online 23 August 2025
1026-9185/© 2025 The Author(s). Published by Elsevier B.V. on behalf of South African Institution of Chemical Engineers. This is an open access article under the CC BY-NC-ND license (http://creativecommons.org/licenses/by-nc-nd/4.0/).

Health Organization (WHO) and 4 mg/L by the Tanzania Bureau of Standards (TBS). These include adsorption (Ku and Chiou, 2002; Zhou et al., 2019), ion-exchange (Waghmare and Arfin, 2015), reverse osmosis (RO) (Dubey et al., 2018; Fritzmann et al., 2007), membrane technology (Ayoob et al., 2008), electrodialysis (Mohapatra, 2009), coagulation (Emamjomeh et al., 2011) and capacitive deionization (CDI), which is facilitated by electric potentials that enhance the migration of ions to the surface of electrodes (Bharath et al., 2021; Rambabu et al., 2020).

In comparison to other conventional techniques, CDI is a cost-effective, fast, and environmentally benign method for water treatment. It does not produce secondary pollutants to the environment. Its performance depends on the influence of factors such as flow rate, applied voltage, cell configuration, feed composition, and electrode materials, which determine how charges are stored on the polarized surface. The performance of the CDI depends on the kind of electrode materials used (Qina et al., 2019).

Different materials have been used in developing electrodes for CDI electrosorption, like activated carbon (AC) (Yeh et al., 2015), carbon nanotubes (CNT) (Cho et al., 2019), carbon aerogels (Liu et al., 2019), carbon nanofibers (Lal and Sundara, 2022) and graphene (Zhang et al., 2020). In this case, AC becomes a very promising electrode material for CDI since it has a good internal structure, well-developed surface area, is environment-friendly, and is commercially available more than CNT, carbon aerogels, nanofibers, and graphene (Choi et al., 2024).

AC can be derived from available biomass materials through activation and carbonization processes (Porada et al., 2013). The AC produced from biomass plants (natural sources) has been pronounced as a suitable material for CDI electrodes because they are cost-effective, efficient, and have excellent properties for electrosorption, sustainability, and renewability (Chen et al., 2011). For example, Elisadiki et al. (2019a) used jackfruit peels to prepare the activated carbon-based electrodes for water desalination. Zhang et al. (2018) reported the preparation of porous carbon with a 3D honeycomb–like electrode using corn-cob through hydrothermal carbonization and KOH activating agent, and applied it for the removal of heavy metals from water. Additionally, biomass-based activated carbon has been extensively studied as an electrode material for CDI for water defluoridation purposes. Biomass-based materials studied with promising results for application in CDI include Douglas-fir (Staphanie et al., 2021), Waste cattail (Dong et al., 2021), tea waste (Gaikwad and Balomajumder, 2017), jackfruit peels (Elisadiki et al., 2020), to mention a few.

In this study, water hyacinths have been selected because they form porous AC with desirable properties for maximum adsorption of charged ions, as they are rich in lignocellulosic materials (Morales et al., 2021; Liang et al., 2018). Water hyacinth plants are locally available in nearly all ponds, rivers, and lakes, posing a threat to aquatic life and contributing to water pollution. They form very dense and impenetrable floating cloud-like mats on the surface of water, causing considerable problems in water ecosystems. Using water hyacinths in the production of activated carbon-based electrodes promotes strategies for controlling water pollution by reducing greenhouse gas emissions, providing an alternative to electrodes made from fossil materials. Therefore, it is advantageous to use these water hyacinths to make CDI electrodes to keep the aquatic environment safe (Liang et al., 2018; Sharma and Aggarwal, 2020).

2. Materials and methods

2.1. Materials

Water hyacinth plants collected from Lake Victoria were used to synthesize activated carbon (AC) and to fabricate electrodes for water defluoridation. Chemicals including concentrated hydrochloric acid used for washing the activated carbon electrode and removing any inorganic materials, activating agent KOH, the source of fluoride ions NaF salt, polytetrafluoroethylene (PTFE) used as binder, carbon black used as additives in water hyacinth AC so as to increase electroconductivity of the electrodes and ethanol were used in fabrication of electrodes, sodium hydroxide (NaOH) used in regulating the pH of water during determination of initial concentration of fluoride in raw water. Sodium chloride, glacial acetic acid, and cyclohexanediaminetetraacetic acid (CDTA) were used to prepare the total ionic strength buffer (TISAB) solution, and ethylenediaminetetraacetic acid (EDTA) was used in the determination of water hardness. All chemicals used were purchased from Sigma-Aldrich and were of analytical grade, used without further purification.

2.2. Preparation of water hyacinth-activated carbon (WHAC)

The water hyacinth samples were washed using raw water to remove impurities attached to the water hyacinth plants. Distilled water was used to clean the water hyacinth, removing sand and some inorganic particles that might have attached to it. Next, the samples were cut into small pieces, dried in sunlight for two weeks, and then placed in an oven at 100 °C for 12 h for complete drying. The dried water hyacinths were ground into powder and labeled WH. Lastly, the WH samples were temporarily stored in the desiccators for further use (Barbosa and Pacheco, 2021).

The 10 g of WH in the ceramic boat crucible was carbonized at 400 °C at a rate of 20 °C per minute for 1 h in a horizontal tube furnace (OTF-1200X from MTI Corporation) under inert conditions of nitrogen gas (35 kPa). The char was assigned the name Carbonized Water Hyacinth (CWH-400). This carbonization temperature was necessary to remove volatile matter from the WH plants and conserve the carbon yield during activation at higher temperatures. Additionally, at this temperature, there is sufficient thermal energy to initiate the formation of a porous structure, which is essential for electrosorption applications (Kaiwen et al., 2017). Five grams of CWH-400 was mixed with 5 M potassium hydroxide and stirred at 80 °C/min for 2 h using an orbital shaker, then dried in an oven at 100 °C for 6 h. The activation was performed using KOH because it plays a significant role in enhancing the porosity and electrochemical conductivity of the material, including the specific surface area and specific capacitance, which are crucial for achieving good electrosorption effectiveness. The dried mixture was activated at a temperature of 500 °C, increasing at 20 °C per minute, for 1 h in the tube furnace under inert conditions. The sample was cooled naturally without being removed from the furnace. All inorganic materials were removed by washing the sample with hydrochloric acid, thereby opening the pores. Then, deionized water was used to remove chlorine from the sample. This process was repeated until the effluents reached a pH of 7, followed by drying the sample in an oven at 100 °C for 12 h. The same procedure was used for the temperatures of 600 and 700 °C. These activation temperatures were used to determine the optimum temperature at which the AC with desired properties is formed. The activated carbons were labeled according to their activation temperature as CWH-400, WHAC-500, WHAC-600, and WHAC-700. The WHAC above 700 °C was not formed during the activation stage using KOH as the activating agent. This may be caused by excessive burn-off, which results in the complete oxidation of the carbon, leading to low yield or no AC left, as it might turn to ash. Also, high temperatures can cause the carbon structure to collapse. The porous structure of the AC formed during carbonization and activation can collapse due to high temperature, leading to the reduction of its porosity and, hence, its effectiveness as activated carbon (Elisadiki, et al., 2019a).

2.3. Characterization of WHAC

2.3.1. Porosity

Automated gas sorption was used to measure nitrogen adsorption and desorption at a temperature of liquid nitrogen (77 K). The specific surface area of the WHAC was ascertained using the Brunauer-Emmett-

Teller (BET) method. The Barrett-Joyner-Halenda (BJH) method was used to analyze the pore size distribution (Sufiani et al., 2023).

2.3.2. Morphology

A scanning electron microscope (SEM) was used to visualize the morphology of water hyacinth-activated carbon at different temperatures (400, 500, 600, and 700 °C) by looking at the particle size, area, and volume (Alfredy, et al., 2022).

2.3.3. Elemental analysis

The elemental analysis was performed using a coupled scanning electron microscope (SEM) equipped with an energy-dispersive X-ray spectrometer (EDX), referred to as SEM-EDX. The elemental analysis of the prepared AC and the CWH aimed to determine the chemical composition of the samples under analysis. This will help to know whether the activation was effective or not, which was then followed by washing the samples with distilled water.

2.3.4. Moisture content

5 g of raw carbon of WH was weighed on the electronic balance labeled m_1 and placed in an oven and dried at 120 °C for 2 h, and the mass was recorded every 10 min until there was no change in weight observed (Mihayo et al., 2022). The final weight was labeled m_2, and the moisture content was obtained using Eq. (1).

$$\% \text{ Moisture content} = \frac{m_1 - m_2}{m_1} \times 100 \quad (1)$$

Where m_1 and m_2 are the initial and final mass of the WH respectively.

2.3.5. Activated carbon yield

This indicates the quality of carbonaceous material in terms of how much AC can be produced from the specified amount of raw materials. The total AC yield was determined after processing the raw material by mass. Six grams of the dried WH powder (W1) were weighed on an analytical balance before carbonization, and then carbonized to obtain the char. After carbonization at 400 °C, the activation process followed (Barbosa and Pacheco, 2021; Mihayo et al., 2022). At each activation temperature, the weight was recorded as W_2, and the total mass of AC yield was determined using Eq. (2):

$$\% \text{ Activated carbon yield} = \frac{\text{Final weight } (W_2)}{\text{Initial weight } (W_1)} \times 100 \quad (2)$$

2.3.6. XRD analysis

The diffraction patterns of WHAC were examined using a Bruker AXS D2 phaser A26-X1-A2B0D2C XRD machine at a wavelength of 1.54060 Å in the Bragg angle (2θ) range from 5° to 80° The Bragg's equation was used to calculate the interlayer spacing using Eq. (3). The Debye-Scherrer equation was used to calculate the microcrystallinity using Eq. (4).

$$n\lambda = 2d\sin\theta \quad (3)$$

$$L_{c,a} = K\lambda/\beta_{c,a}Cos\theta \quad (4)$$

From Eqs. (3) and (4); n represents the order of reflection, λ is the X-ray wavelength, equal to 1.54060 Å; θ represents the position of the diffraction peaks at the plane indices of 002 and 100. L_c and L_a represent the stack height and width, respectively, and K represents the shape factor, which is equal to 0.89 and 1.84 for L_c and L_a, respectively. $\beta_{c,a}$ represents the full width at half maximum of the symmetrically shaped diffraction peaks (Alfredy, et al., 2023; Elisadiki, et al., 2019a).

2.3.7. Functional group analysis

Fourier Transform Infrared Spectroscopy (FTIR) analysis was done to identify the transmittance spectrum of the samples and the functional groups presented on the surface of the WH sample before carbonization, in CWH, and in activated carbon at the wave number measurement ranging from 500 to 4000 cm^{-1} (Mihayo et al., 2022).

2.4. Fabrication of CDI electrodes

The water hyacinth-activated carbon (WHAC) was used to fabricate the electrodes, which were formed by mixing activated carbon (AC), conducting carbon, and PTFE in an 8:1:1 ratio, respectively. 15 mL of ethanol (99.9 %) was added to the mixture and stirred using a magnetic orbital shaker at 100 rpm for 30 min, until a paste formed. The paste was squeezed to form an electrode with dimensions of 4 cm x 4 cm and a thickness of 1 mm, and then dried at 80 °C for 12 h using a vacuum oven. The electrodes were ready to be assembled in the CDI cell for the electrosorption experiments (Alfredy et al., 2022; Rambabu et al., 2020). The fabrication process of electrodes from WH is shown in Fig. 1.

2.5. Electrochemical properties of the electrodes fabricated using cyclic voltammetry

The electrochemical properties of WH electrodes were investigated using an electrochemical workstation with a three-electrode system, where a reference, counter, and working electrode were employed. The reference electrode used was a saturated Ag/AgCl (KCl). Platinum wire was used as the counter electrode. The working electrode, with a 1 cm x 1 cm dimension, was prepared by mixing AC, carbon black, and PTFE binder in an 8:1:1 ratio and then folded onto a nickel foam, which served as the current collector. Cyclic voltammetry was used to investigate the electrochemical behavior of the electrodes in a 6 M KOH solution using an electrochemical workstation. The cyclic voltametric analysis was carried out using a potential window range of 0–1 V at different scan rates, and then the voltammogram was drawn (Rambabu et al., 2020).

The area under the cyclic voltammograms is the capacitance of the electrode. Specific capacitance (C_{sp}) was determined using Eq. (5):

$$C_{sp} = \frac{\int IdV}{2 \times m \times \Delta V \times S} \quad (5)$$

Where ∫IdV is the area under the cyclic voltammograms, S is the scan rate (mV/s), m is the mass (g) of the electrode, and ΔV is the voltage (V) (Dong et al., 2021).

2.6. Defluoridation experiments

Before the electrosorption experiments, the collected water samples were analyzed for their physicochemical parameters, including pH, electrical conductivity (EC) in μS/cm, and total dissolved solids (TDS), which were measured using a multi-parameter analyzer. The complexometric method was used to determine the total hardness of water in terms of Ca-$CaCO_3$ using EDTA with Eriochrome black T as an indicator, along with ammonium buffer. Fluoride ions were measured by mixing the total ionic strength buffer (TISAB) in the mixing ratio of 1:1. TISAB was prepared by mixing 58 g sodium chloride (NaCl), 57.0 mL glacial

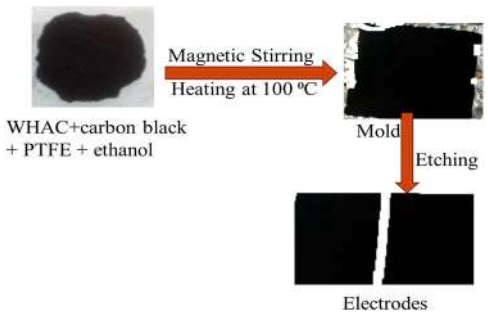

Fig. 1. The fabrication of WHAC-based electrodes.

acetic acid, and 4 g of CDTA in 500 mL of distilled water. A 20 mL water sample and 20 mL of TISAB were mixed and stirred for 5 min using a magnetic stirrer. A fluoride ion-selective electrode (ISE) was then placed in the solution mixture to measure the concentration of fluoride ions in the water. Before the measurement, the solution's pH was adjusted to neutral by using a 6 M NaOH solution (Elisadiki et al., 2019c).

Electrosorption experiments were conducted to determine the amount of fluoride electrosorbed onto the electrodes. The 10 cm x 10 cm CDI cell was connected to a power supply, a peristaltic pump that facilitated the water flow, a feed tank, a pH meter, and a conductivity meter to make a complete experimental setup. The 4 cm x 4 cm electrodes in the titanium sheet current collectors were placed in the CDI cell. A 1 mm plastic mesh was used to separate the two electrodes, allowing for unidirectional water flow and inhibiting short circuits within the cell system. The gaskets were placed between to seal the cell and prevent side flow of solution, and the whole system's components were covered using Plexiglas and strengthened with screws (Elisadiki et al., 2019b).

The CDI cell voltage was supplied by a potentiostat (CS350) during electrosorption experiments. This cell voltage helped identify the optimal voltage and charging time for electrosorption to be more efficient. In electrosorption experiments, 50 mL of a water solution with varying concentrations (from 3 mg/L to 15 mg/L) was passed into the CDI cell using a peristaltic pump and circulated into the feed tank at a flow rate of 10 mL/min.

Then, the removal efficiency of fluoride by the CDI cell can be calculated using Eq. (6).

$$\%\ \text{Fluoride removal} = \frac{C_o - C_f}{\text{Co}} \times\ 100 \tag{6}$$

Where C_0 is the initial fluoride concentration before treatment using the CDI cell, and C_f is the final fluoride concentration after treatment (Dong et al., 2021).

2.7. Reusability of the WHAC electrodes

The regeneration experiments were conducted using water hyacinth-activated carbon (WHAC) electrodes, which show excellent performance in all water samples. The electrode used was regenerated by reversing the cell terminals. After regeneration, it is again used for removing fluoride. This process is repeated for five cycles. After every cycle, the fluoride concentration was measured and recorded (Alfredy et al., 2023).

3. Results and discussion

3.1. Physical and chemical characterization of WHAC

3.1.1. Porosity

Nitrogen adsorption-desorption isotherm plots of the resulting activated carbons are shown in Fig. 2. The results indicate that the volume adsorbed increases from CWH-400 to WHAC-700, signifying an improvement in the specific surface area and pore volume of the activated carbon. It was observed that sample WHAC-700 exhibited a high N_2 adsorption capacity, with a specific surface area of 1020.01 m^2/g, as presented in Table 1. The N_2 adsorption plot shows a linear increase in its gradient as the activation temperature increases from 400 °C to 700 °C, indicating that the activated carbon develops porous properties due to the formation of new pores during activation with increasing activation temperature. The carbonized sample exhibited low nitrogen adsorption, indicating that the water hyacinth material underwent incomplete carbonization, a finding consistent with that reported by Elisadiki et al. (2019a). It has been observed that as the activation temperature increased to 700 °C, the volumes adsorbed also increased, indicating that the AC has developed more new pores. At lower relative pressure, there was no abrupt uptake of N_2vol, signifying that the AC synthesized has only a small amount of micropores. In comparison, at higher relative pressures, there was a greater uptake of N_2vol, indicating the presence of a minimal number of mesopores in WHAC, consistent with the findings reported by Zornitta et al. (2017) and Elisadiki et al. (2019a).

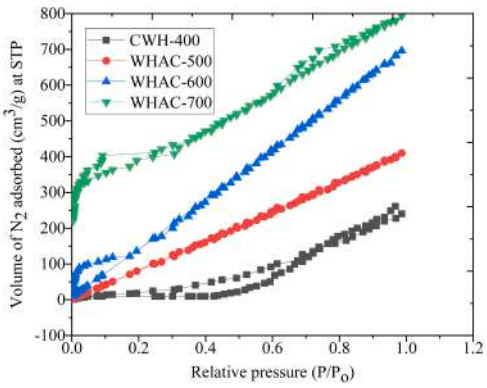

Fig. 2. Nitrogen adsorption/desorption isotherms of WHAC.

Table 1
Porosity of WHAC with increasing activation temperature.

Sample	Pore size (nm)	Specific surface area (m^2/g)	Total pore volume (cm^3/g)
CWH-400	7.61	464.67	0.13
WHAC-500	7.72	650.75	0.16
WHAC-600	7.90	967.22	0.20
WHAC-700	8.06	1020.01	0.25

The pore size distribution of the AC sample was determined from N_2 desorption data with the BJH technique, as indicated in Table 1. It has been observed that the AC synthesized has a pore size in the range of 7.61 to 8.06 nm, indicating that the AC sample contains mesopores. The mesopores contribute to the surface area and provide a large channel for ion transport to micropores; as a result, the electrosorption capacity of the AC is improved, as reported in the research by Noked et al. (2009).

The specific surface area of the AC synthesized was assessed using BET analysis, and the results are presented in Table 1. It has been observed that the activation temperature affects the specific surface area. As the activation temperature increased, the specific surface area also increased. In this research, it has been observed that sample WHAC-700 has a specific surface area of 1020.02 m^2/g, showing the presence of a more porous nature for adsorption that ultimately favors the electrochemical behavior of the AC (Mohanta and Mohanty, 2018; Mohanty et al., 2005; Prahas et al., 2008).

The total pore volume depends on both pore size and specific surface area. The total pore volume increases with an increase in pore size and specific surface area. The same is observed in this study. As the activation temperature increased from 400 to 700 °C, the total pore volume increased from 0.13 to 0.25 cm^3/g (Table 2). This indicates more capacity for the electrosorption process.

Table 2
Percentage of AC yield from WH plants.

Sample	Initial weight (W_1) (g)	Final weight (W_2) (g)	AC yield (%)
CWH-400	6.00	–	–
WHAC-500	6.00	4.81	80.14
WHAC-600	6.00	3.21	53.51
WHAC-700	6.00	2.90	48.40

3.1.2. Morphology

The morphology of WHAC samples activated at different temperatures is shown by SEM images in Figs. 3 and 4. It is observed that WHAC at 400 °C developed the non-porous carbons agglomerated together on the surface. Additionally, the carbons produced were found to have block-like structures due to incomplete carbonization resulting from a low activation temperature (Fig. 3(a)), a phenomenon also reported by Huang et al. (2014) and Barbosa et al. (2021). The low carbonization temperature leads to the formation of carbons with limited pores, due to pore blockage, resulting in a low specific surface area and pore volume in the sample materials (Huang et al., 2014). The introduction of an activating agent into the material sample, accompanied by an increase in temperature, resulted in the development of more pores and surface roughness, highlighting the importance of activation temperature on the sample's electrosorption performance. It is observed that the increase in temperature has led to the sample acquiring a rough surface, as shown in Figs. 3(b) to 3(d), particularly at activation temperatures from 500 to 700 °C. The rough surface of the sample is crucial for the electrosorption of ions on the electrode surface, as reported by Matsubara et al. (2010). At low resolution, Figs. 4a-d, it has been observed that the WHAC particles are not closer to each other due to the agglomeration of carbon on their surface. It has been observed that at high resolution, the pores appear to be closer in the AC sample, especially at temperatures of 600 and 700 °C. This is due to the intercalation of potassium into the carbon layers during the activation process as shown in Eq. (8) (Hui and Zaini, 2015; Otowa et al., 1993; Wang and Kaskel, 2012). Eqs. (7)-(13) describe the different reactions that have taken place in the activation process using KOH as an activating agent. Eq. (8) shows the dehydration of KOH into K_2O that was followed by water gas reactions as shown by Eqs. (9)-(11). The carbonates formed in Eq. (7) decomposed into CO_2 and K_2O, which disappeared at activation temperatures higher than or equal to 700 °C activation temperature, as shown in Eq. (13). The reduction of K_2O by carbon gave metallic K, which intercalated in the carbon sample and caused the widening of the carbon layer. The metallic K was removed from the carbon matrix by washing with concentrated hydrochloric acid, followed by distilled water, which resulted in the expansion of the carbon lattices that could not return to their original form; hence, more pores were formed. The results have indicated that the temperature and mixing ratios of KOH and carbon (KOH/C) are crucial factors in evaluating the textural and surface behavior of AC produced from WH plants, consistent with the findings of Wu et al. (2016) and Elisadiki et al. (2019c). Hence, the WHAC produced has demonstrated good capacitance and electrosorption ability due to its large specific surface area, pore size, and pore volume, which are key criteria in selecting CDI electrode materials.

$$6KOH + 2C \rightarrow 2\,K + 3H_2 + 2K_2CO_3 \quad (7)$$

$$2KOH \rightarrow K_2O + H_2O \quad (8)$$

$$C + H_2O \rightarrow CO + H_2 \quad (9)$$

$$CO + H_2O \rightarrow CO_2 + H_2 \quad (10)$$

$$CO_2 + K_2O \rightarrow K_2CO_3 \quad (11)$$

$$K_2CO_3 \rightarrow K_2O + CO_2 \quad (12)$$

$$C + K_2O \rightarrow 2\,K + CO \quad (13)$$

3.1.3. Elemental composition of the AC

The results showed that the carbonized sample (CWH-400) has many elements such as carbon (C- 28.25 %), oxygen (O- 39.95 %), magnesium (Mg- 2.53 %), aluminium (Al- 1.50 %), silicon (Si- 4.07 %), phosphorus (P- 3.70 %), potassium (K- 4.00 %) and calcium (Ca- 15.98) in which oxygen is more predominant in this sample similar to that reported by Boulika et al. (2022) and Erabee et al. (2017). As the carbonization temperature was increased the number of elements decreased meaning that some elements in the sample were not resistant to high temperature and some inorganic metals were removed during washing with concentrated hydrochloric acid as shown in Fig. 5. Potassium element disappeared in sample WHAC-700 during washing that is why no peak was found on the spectrum. Carbon was found to be abundantly present in the sample activated at a temperature of 700 °C, indicating that the sample prepared was amorphous AC, which was used in forming CDI

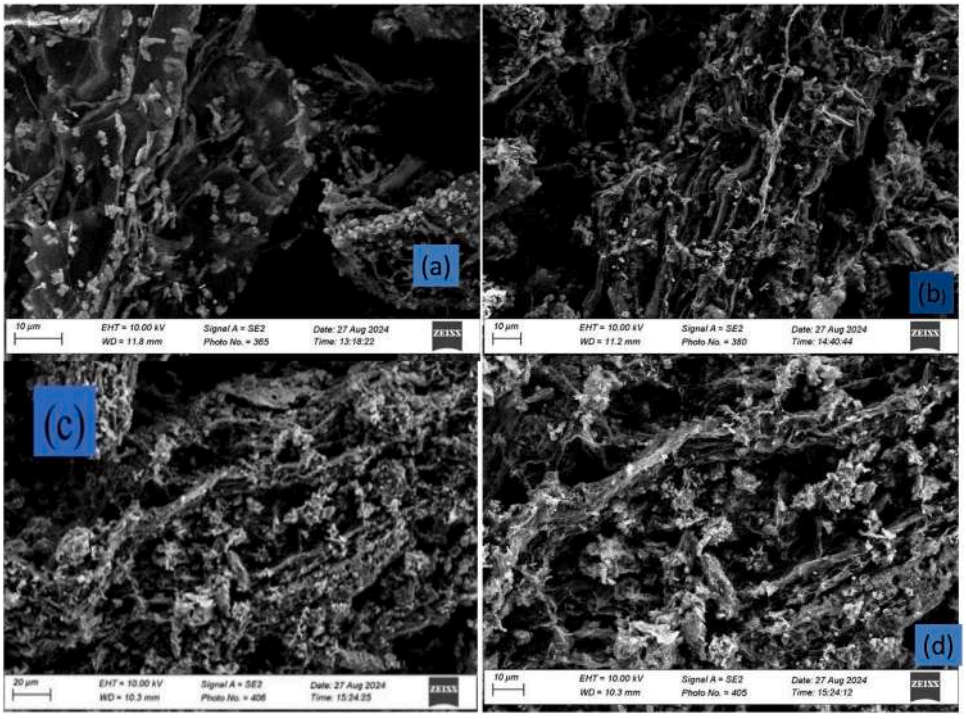

Fig. 3. SEM images (a) CWH-400, (b) WHAC-500, (c) WHAC- 600, and (d) WHAC-700 high resolution.

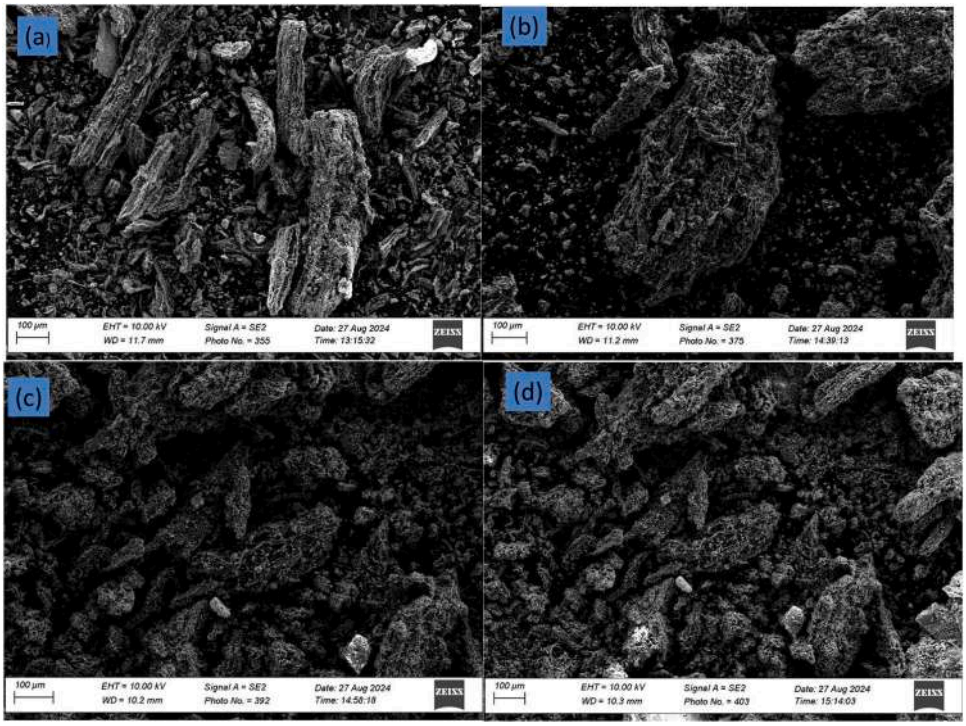

Fig. 4. SEM images (e) CWH-400 (f) WHAC-500 (g) WHAC- 600 (h) WHAC-700 low resolution.

electrodes with high specific capacitance, as supported by cyclic voltammetry in Fig. 9, similar to what Mopoung et al. (2015) reported.

3.1.4. The moisture content

WH plants grow in water and survive in water since they are hydrophytes. Therefore, the water (moisture) content of the resulting carbon was measured to determine if the amount of moisture would have an effect during electrosorption processes. The moisture content of WH samples was calculated using Eq. (1). When the WHAC was subjected to moisture content analysis at different activation temperatures, the results showed a decrease as the activation temperature increased, as shown in Fig. 6. The AC with lower moisture content has higher adsorption performance than that with higher moisture content because of having high specific surface area and high a specific capacitance. Gumus and Okpeku (2015) reported that the moisture content of biomass-based AC required for good adsorption ranges between 3 % and 6 %. Results of WHAC in all activation temperatures are within the literature values, as reported by Gumus and Okpeku (2015) and showed to be near normal based on the American Society of Testing and Materials (ASTM) (Rangari and Chavan, 2017) and also resembles what Mihayo et al. (2022) reported.

3.1.5. AC yield

The AC yield from WH plants was determined at each activation temperature, and the results are indicated in Table 2. The results indicate a decrease in carbon yield as the activation temperature increases. This is because as the activation temperature increases, there is a carbon burn-off promotion and tar volatilization at higher temperatures, resulting in low yield (Sun et al., 2024). The percentage AC yield was calculated using Eq. (2). The AC yield decreases from 80.14 % at an activation temperature of 500 ºC to 48.40 % at an activation temperature of 700 ºC, leading to amorphous carbon with high capacitance and specific surface area (Erabee et al., 2017). These results make the WH plants a suitable activated precursor for use in various scientific processes.

3.1.6. XRD analysis

Fig. 7 indicates the X-ray diffraction patterns of the unactivated carbon (CWH) and AC sample at 700 °C. The presence of two broad peaks at 2θ of 22.76° and 42.56°, which were given index planes of (d002) and (d100), shows that the AC synthesized has amorphous properties, which then gives the assurance that the AC produced from WH plants consists of disordered (turbostratic) structures. However, in the CWH sample, the peaks are not very visible. This could be associated with the presence of impurities or inorganic substances in the carbon precursor, which disappeared during the activation process, and others when washing the sample with HCl. It can be stated that the smaller the crystallinity, the larger the specific surface area of the AC synthesized, as reported by Anton et al. (2016). The XRD structural parameters were calculated from the diffraction pattern data obtained from the X-ray and are indicated in Table 3. It has been observed that the calculated parameters have shown slight variations in the plane d002 and d100 in all four WHAC samples, indicating that the activation temperature and the activating agent to carbon (KOH/C) ratio did not significantly affect the microcrystalline orientation. The results also show that the calculated interlayer spacing in d002 varies from 3.80 to 3.90 Å, which is higher than the graphitic dimensions of 3.35 Å. These results imply that the WHAC carbon synthesized has fully disordered (turbostratic) structures, similar to those described by Girgis et al. (2007) reported. Other parameters calculated from the XRD data were L_c and L_a, as indicated in Table 3. The results have shown a constant value of Lc equal to 18.97 Å, and the value of La has been observed to range from 49.98 to 50.58 Å. The constant ratio of L_c/L_a was found to be 0.37. These microcrystalline size and orientation parameters play a significant role in the formation of the electric double layer and specific capacitance value of the material as reported elsewhere by Nabais et al. (2011).

3.1.7. Functional groups analysis

Fourier Transform Infrared Spectroscopy (FTIR) analysis was done to identify the transmittance spectrum of the samples and the functional groups present on the surface of the WH sample before carbonization, in carbonized WH, and AC at the wave number measurement ranging from 500–4000 cm^{-1} as presented in Fig. 8. The results showed that the

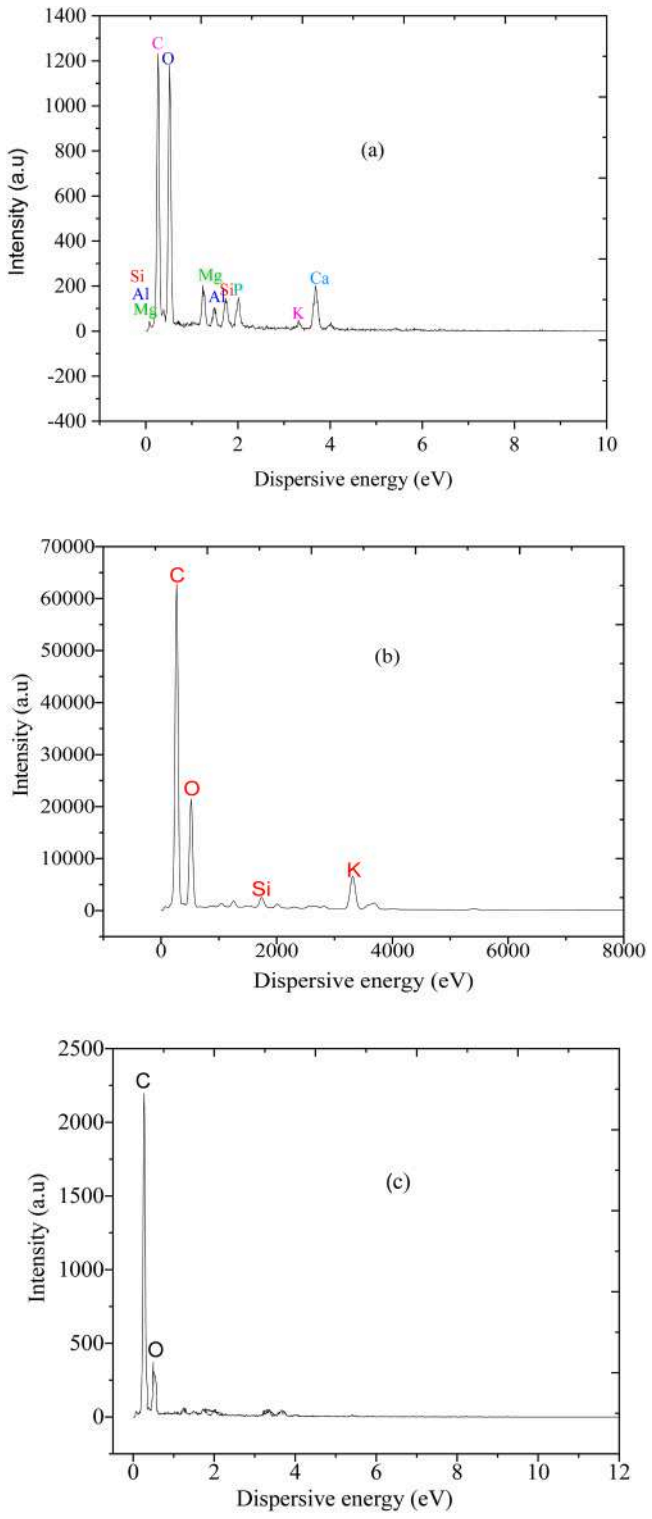

Fig. 5. EDX analysis of (a) CWH-400, (b) WHAC-600, and (c) WHAC-700.

sample before carbonization had other organic substances that were identified through their functional groups as presented in Fig. 8. The functional groups observed on the spectrum are 3333.40 cm^{-1} suggesting a strong O—H stretching band, which indicates hydrogen bonding. The peak at 1604.07 cm^{-1} corresponds to the stretching vibration of the carbon-carbon double bond ($C = C$) in an aromatic ring or conjugated alkene. The peak at 1319.06 cm^{-1} corresponds to the C—O stretching vibrations in alcohols, phenols, or carboxylic acids. The peak at 1033.06 cm^{-1} corresponds to the bending vibration of the C—O bond in an

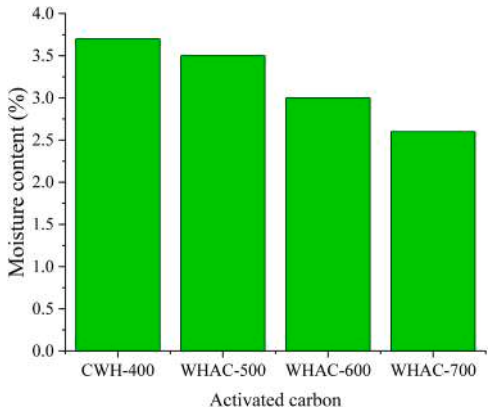

Fig. 6. Moisture content of AC.

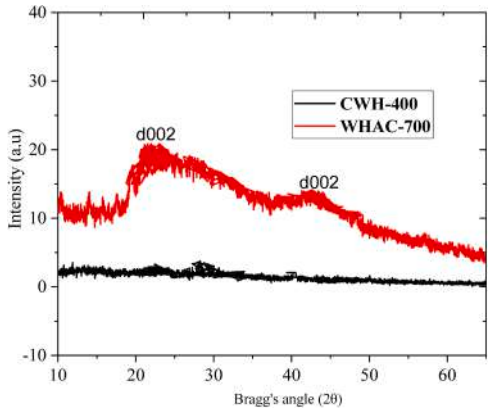

Fig. 7. The diffraction patterns of WHAC at 400 °C and 700 °C.

Table 3
Interlayer d-spacing, microcrystalline dimension, and ratios of L_c/L_a and Np in all the samples.

Sample	Interlayer d-spacing (Å)		Microcrystalline dimension (Å)			
	d002	d100	Lc	La	Lc/La	Np
CWH-400	3.80	2.08	18.97	49.98	0.38	4.99
WHAC-500	3.86	2.09	18.97	50.37	0.37	4.91
WHAC-600	3.88	2.10	18.97	50.42	0.37	4.89
WHAC-700	3.90	2.12	18.97	50.58	0.37	4.86

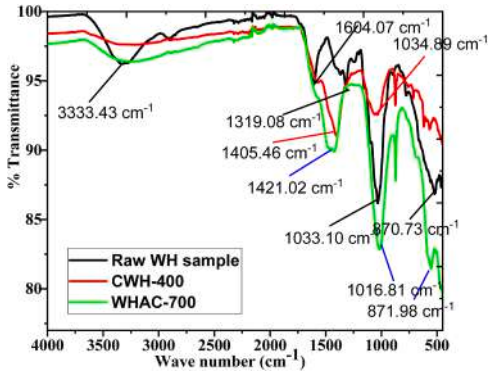

Fig. 8. FT-IR analysis of water hyacinth samples in WH powder (Raw WH sample), Carbonized WH powder at 400 °C (CWH-400), and activated WH at 700 °C (WHAC-700).

alcohol (R-OH) or ether (R-O-R') functional group. This absorption is characteristic of the ether linkage (-C-O—C-) or the hydroxyl group (-OH) in alcohols. These functional groups often exhibit absorption in the range of 1030–1080 cm^{-1} due to the stretching vibration of the C—O bond. The peak at 870.73 cm^{-1} corresponds to the out-of-plane C—H bending of aromatic rings, suggesting the presence of either isolated or disubstituted aromatic groups in the WH sample. In a carbonized CWH-400, the dimerization of the carboxylic group was evidenced by the presence of the extension of the peak from around 2500–3600 cm^{-1}. The peak at 1405.46 cm^{-1} indicated the presence of C—H bending vibrations in methyl or methylene groups. Additionally, this peak may be associated with the symmetric stretching of the carboxylate group (COO^-). The peak at 1034.89 cm^{-1} corresponds to the C—O stretching vibration in alcohols or ethers.

The WHAC-700 showed the extension of the peak from 2500 – 3600 cm^{-1}, which may have been caused by the dimerization of the carboxylate group during the activation process. The peak at 1421.02 cm^{-1} was attributed to the C—C stretching vibration in aromatic rings, resulting from the increase in aromatization due to temperature during activation, or it may be due to C—O symmetric stretching in carboxylates. The peak at 1016.81 cm^{-1} corresponds to C—O stretching vibrations in alcohols, ethers, or esters. The peak at 871.98 cm^{-1} was attributed to C—H out-of-plane bending of aromatic rings, which occurred due to aromatization resulting from the activation temperature. This indicated an increase in the high number of carbons, which ultimately provided evidence that the formed material is amorphous in nature, as supported by the results from X-ray diffractograms in Fig. 7 and the EDX results presented in Fig. 5.

It has been observed that the WH sample results showed that the functional groups on the sample were dispersed in such a way that they were not close to each other. Commonly, plant residues are composed of almost the same functional groups, such as carboxyl, phenol, quinones, and lactones, that can bind pollutants to some extent. The WHAC-700 results in Fig. 8 show the effect of temperature on the activated WH samples. As the temperature increased, the functional groups in the sample were lost, showing that activation temperature plays a vital role in the preparation of AC (Zhao et al., 2017). Also, it was found that the aromatization increased as the temperature increased, which is evident on the spectrum due to the increase in -CH bending vibrations at the wave number ranging from 1400 cm^{-1} to 800 $cm^{-1,}$ similar to what was reported elsewhere by Barbosa & Pacheco (2021).

3.2. Electrochemical characterization of fabricated electrodes

The electrochemical performance of the WHAC-based electrodes was studied using cyclic voltammetry (CV) to investigate the electrical double layer (EDL) formed on the electrode surface due to its reasonable working principle of CDI (Li et al., 2010). The EDL properties of the fabricated WHAC electrodes were tested using CV, as indicated in Fig. 9. The shapes of voltammograms are nearly quasi-rectangular with no reduction/oxidation peaks observed. This indicated that the fluoride ions were removed by EDL, consistent with the findings of Bharath et al. (2021) and Yang et al. (2020).

The specific capacitances (C_{sp}) are presented in Figs. 10 and 11 were calculated using Eq. (5). The results revealed that the specific capacitance decreased as the scan rate increased, as indicated in Fig. 10, which shows that the scan rate is inversely proportional to specific capacitance, as reported elsewhere by Quach et al. (2017). Because at low scan rates, the ions get more time to interact with the active pores of WHAC, making the migration of ions and finally higher capacitance at low scan rates, compared to high scan rates (Alfredy et al., 2023; Yasin et al., 2018). The specific capacitance was found to be 501.86 F/g at a scan rate of 5 mV/s. The enhanced specific capacitance can be attributed to the fact that, with an increase in activation temperature, the electrical resistance of WHAC is reduced, making charge transfer easier. Additionally, the improved specific capacitance of WHAC-700 is attributed to

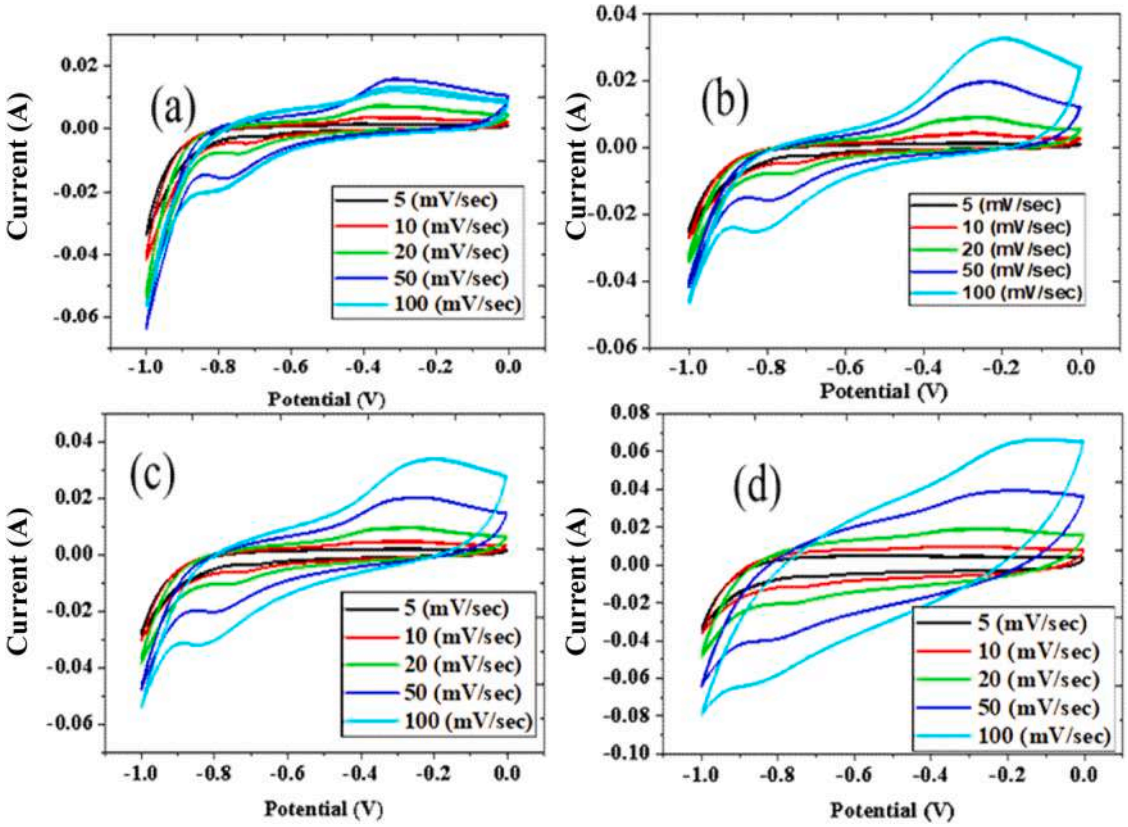

Fig. 9. Cyclic voltammograms of (a) CWH-400 (b) WHAC-500 (c) WHAC-600 and (d) WHAC-700.

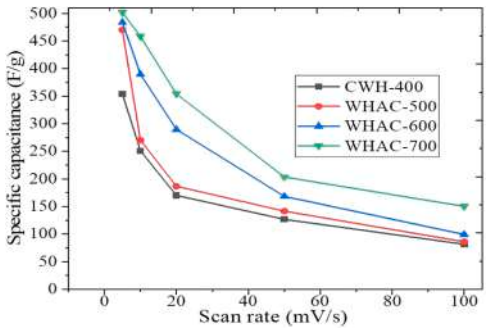

Fig. 10. Specific capacitance of water hyacinth-activated carbon with respect to scan rates in CV measurements.

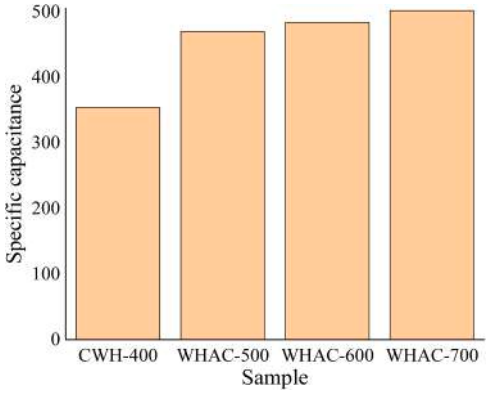

Fig. 11. The specific capacitance of WHAC at different temperatures at a scan rate of 5 mV/*sec*.

its richer porosity and higher specific surface area, which are developed at higher activation temperatures, as shown in Table 1 for porosity analysis. Specifically, at WHAC-700, pore formation was high, resulting in a high specific surface area. The results have shown that the specific capacitance of the WHAC-based electrodes increased as the activation temperature was increased (Fig. 11), similar to what has been reported elsewhere by (Adinaveen et al., 2013). This finding is in agreement with the results obtained in this research, where WHAC-700 exhibited the largest BET surface area and the highest specific capacitance. It has been observed that specific capacitance is directly proportional to the specific surface area. Based on the results obtained, WHAC is not only used for CDI but also as a good electrode material in supercapacitors.

3.3. Defluoridation experiments

3.3.1. Water characterization

The measured physicochemical parameters are shown in Table 4 for water samples A, B, and C, respectively. Water samples were characterized to identify other water components apart from fluoride that may hinder the electro-sorption of fluoride. The water samples collected from their sources, as specified, contained other mineral ions that competed with fluoride ions on the active sites during electrosorption on the WHAC electrodes. This analysis revealed that all water samples contained other contaminants within the recommended amounts set by the WHO, except for fluoride, which was found to be higher than the proposed 1.5 mg/L limit. So, the water composition has been found to reduce the fluoride sorption on the active sites of the electrodes due to the competing effect of other existing ions, similar to what was reported by Alfredy et al. (2022) and Tang et al. (2026). It is also evident that the decrease in defluoridation is caused by the water components (anions) such as chlorine (Cl^-), sulphate (SO_4^{2-}), nitrate (NO_3^-), and hydrogen carbonate (HCO_3^-), since the collected water samples contain these ions (Zhan et al., 2021).

3.3.2. Electrosorption experiments

The electrosorption mechanism of the WHAC electrode in removing ions in water is based on adsorption of ions in a double layer formed due to applied potential similar to the working mechanism in supercapacitors, though the CDI aims at adsorbing the ions from water and not energy storage (Elisadiki et al., 2019c; Leong and Yang, 2020). When potential energy is applied, the ions in water are attracted and adsorbed into the double layer, where they are removed from the water by the electrosorption process. The adsorbed ions in the double layer are released back into the water by reversing the circuit's terminals.

To investigate the electrosorption behavior of the WHAC electrodes, prior experiments were conducted using a NaF solution with known concentrations, starting with 3, 5, and 10 mg/L, to validate the efficiency of the fabricated WHAC electrodes for their applicability in different water samples with varying fluoride concentrations. The cell voltages used during these experiments were 1.2, 1.4, and 2.0 V. The results for 3, 5, and 10 mg/L were found to be 73.67, 74.40, and 77.90 %, respectively, with the average of 75.32 % working efficiency of the electrodes at the applied potential of 2.0 V in a charging time of 180 min with a flow rate of 10 mL/min as shown in Table 5.

Electrosorption experiments were also conducted to investigate the electrosorption capacity of WHAC electrodes fabricated using water samples collected from three different sources. The three-dimensional plots were created using Box-Behnken to illustrate the mutual effect of each parameter during water defluoridation, as shown in Figs. 12a, 12b, and 12c (Mihayo et al., 2021).

Water sample A was found to have an initial electroconductivity of 461.75 μS/cm and a fluoride concentration of 4.21 mg/L. During defluoridation experiments, it was found that the electroconductivity decreased sharply within the first 30 min, reaching 338.18 μS/cm, and then further decreased to 255.98 μS/cm after a charging time of 180 min. These results implied the defluoridation process to take place efficiently using WHAC-700, in which the fluoride concentration was reduced from 4.21 mg/L up to 1.28 mg/L, which is below the

Table 5
Electrosorption results for NaF solution at a cell voltage of 2.0 V.

Experiment	Initial (C_o)	Final (C_f)	Removal Efficiency (%)
Amount of fluoride (mol/L)	10	2.21	77.90
	5	1.28	74.40
	3	0.79	73.67
Average efficiency (%)			75.32

Table 4
Physicochemical parameters of water samples A, B, and C.

Parameter	pH	EC (μS/cm)	TDS (ppm)	F (mg/L)	Ca^{2+}(mg/L)	Mg^{2+}(mg/L)	NO_3^-(mg/L)	Cl^-(mg/L)	HCO_3^-(mg/L)	SO_4^{2-} (mg/L)
Water sample A										
Amount	6.98	461.75	238.25	4.21	38.54	13.21	7.60	27.18	252	15.50
Water sample B										
Amount	7.23	487.21	245.61	4.61	27.80	12.93	1.00	67.36	258.03	29.56
Water sample C										
Amount	6.56	456.01	230.25	3.51	16.37	11.67	6.21	14.32	190.00	15.11

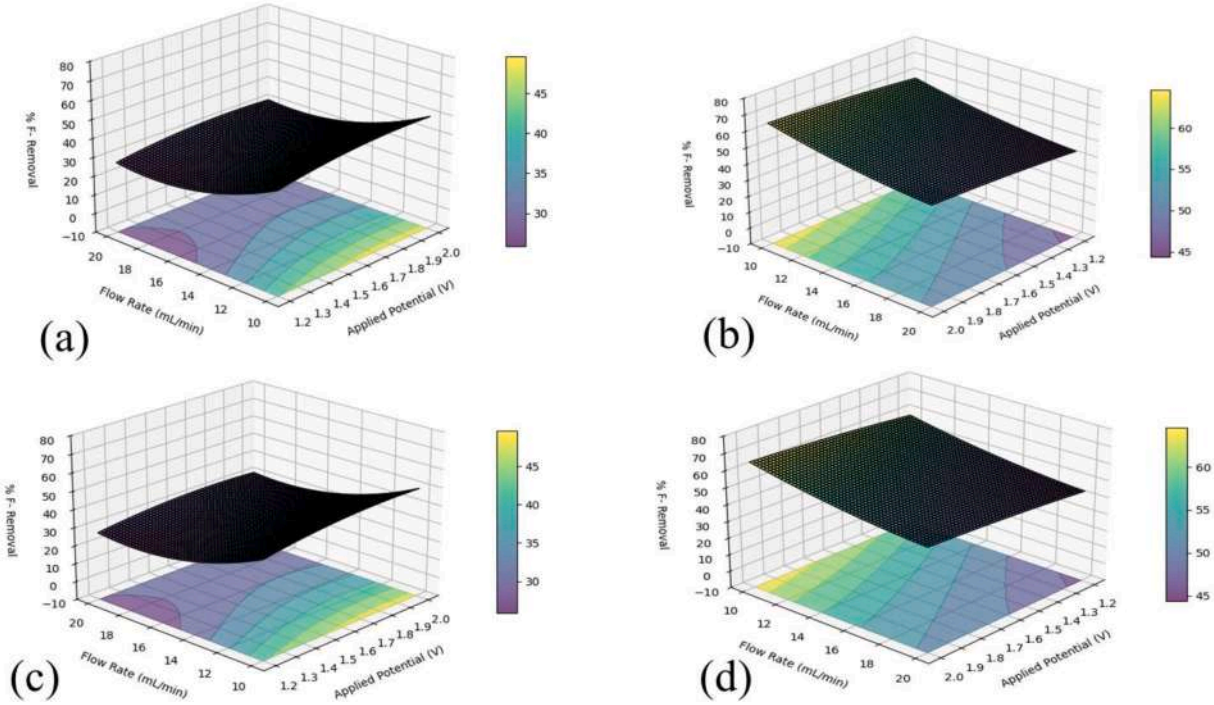

Fig. 12a. WHAC electrodes efficiency for water sample A (a) CWH-400 (b) WHAC-500 (c) WHAC-600 (d) WHAC-700.

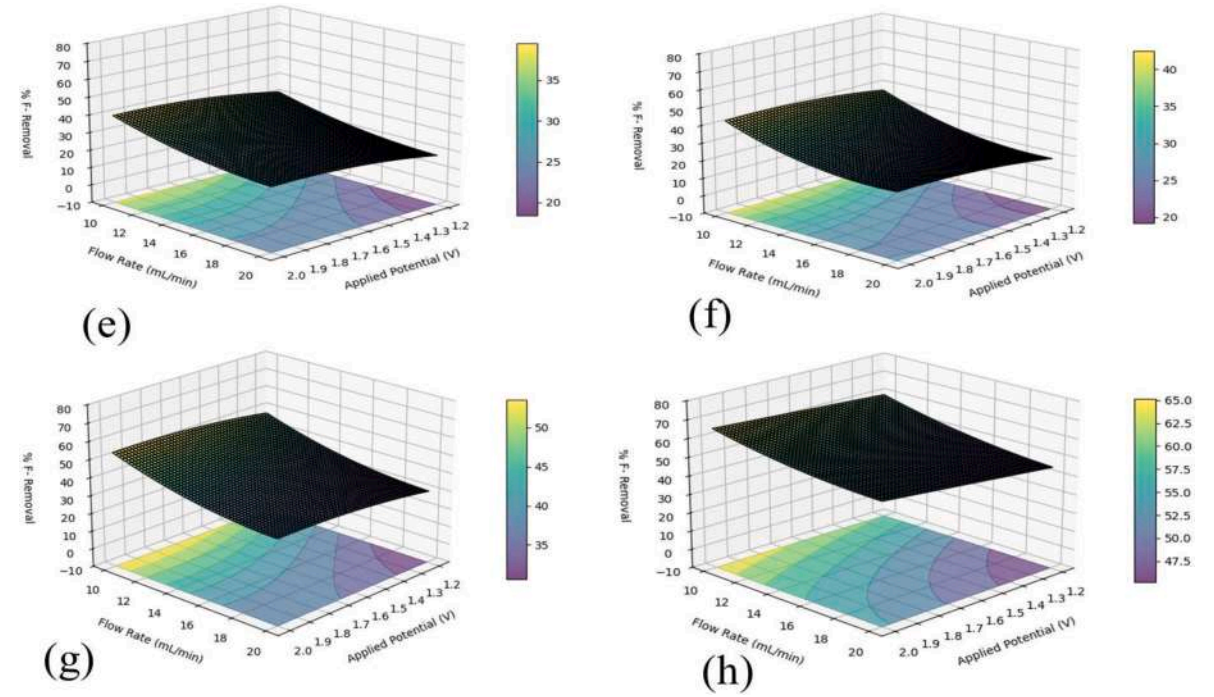

Fig. 12b. WHAC electrodes efficiency in water sample B (e) CWH-400 (f) WHAC-500 (g) WHAC-600 (h) WHAC-700.

recommended amount of 1.5 mg/L (WHO, 2019) When 2.0 V was applied, a potential was used at a flow rate of 10 mL/min and a charging time of 180 min. It was also noted that the defluoridation was enhanced by factors such as charging time, flow rate, and applied potential. The results showed that at low flow rates and high applied potential, the defluoridation was increased, as shown in Fig. 12a. This is because at low flow rate, the water sample got much contact time to complete the defluoridation process as compared to higher flow rate which used little time to contact with the active sites of the electrodes. (Alfredy et al., 2022). At higher applied potential, the electric current created a strong electric double layer that facilitated more fluoride ions to be electrosorbed on the surface of the electrodes, similar to what was reported elsewhere by Foo and Hameed (2009) and Elisadiki et al. (2019b). The highest electrosorption efficiency of 69.60 % was achieved using WHAC-700 at a flow rate of 10 mL/min and an applied potential of 2.0 V for 180 min in water sample A.

Water sample B was initially found to have a fluoride concentration of 4.61 mg/L and an electroconductivity of 487.21 μS/cm. It was found

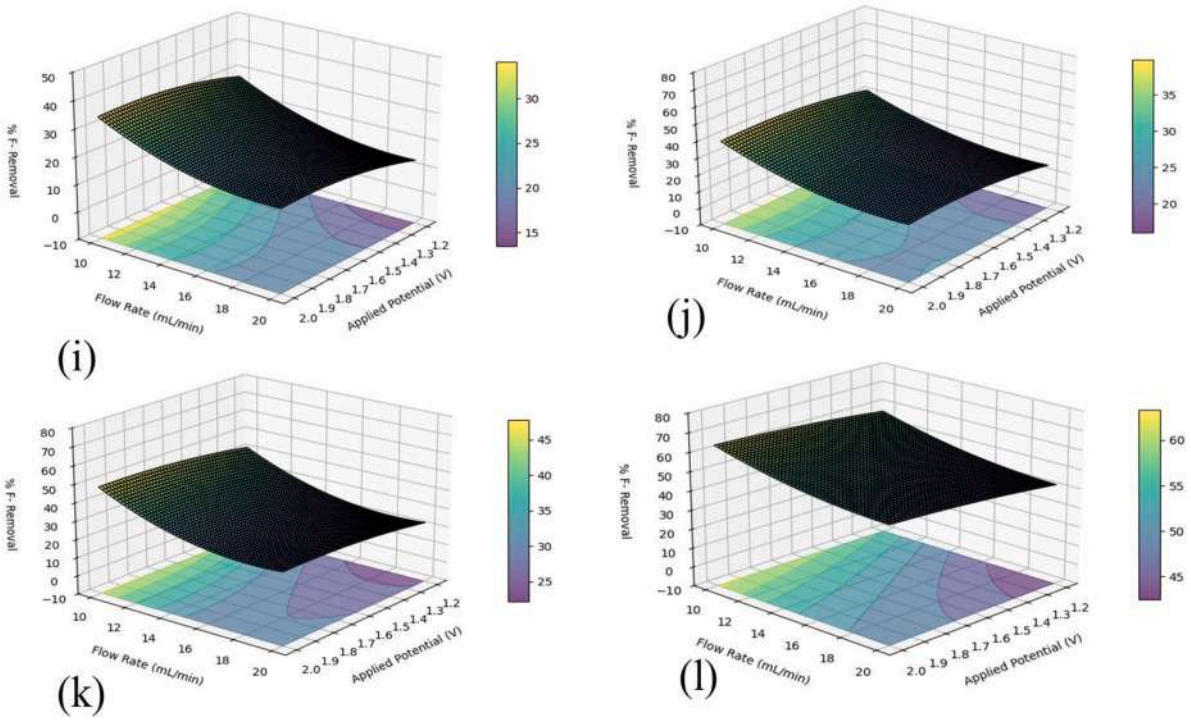

Fig. 12c. WHAC electrodes efficiency in water sample C (i) CWH-400 (j) WHAC-500 (k) WHAC-600 (l) WHAC-700.

that the electroconductivity decreased sharply in the first 30 min of the defluoridation process, with a conductivity decrease of up to 336.95 μS/cm. The defluoridation experiment results showed that electroconductivity was found to decrease up to 254.75 μS/cm at a charging time of 180 min, where the fluoride concentration was reduced to 1.37 mg/L, which is below the amount of 1.5 mg/L as suggested by WHO (2019) at a charging time of 180 min and a flow rate of 10 mL/minute when 2.0 V was applied. Again, the results obtained were influenced by multiple factors, such as charging time, flow rate, and applied potential, as shown in Fig. 12b The results indicated that defluoridation increased at low flow rates and high applied potentials. This is because at a low flow rate, the water sample had more time to complete the defluoridation process as compared to a higher flow rate, which used a short time to contact the active sites of the electrodes. At higher applied potentials, the electric current created a strong electric double layer, which facilitated an increase in the strength of the electric double layer (EDL). Hence, more fluoride ions were electrosorbed onto the surface of the electrodes. The highest electrosorption efficiency of 70.28 % was obtained using WHAC-700 at a flow rate of 10 mL/min and an applied potential of 2.0 V for water sample B.

Water sample C was initially found to have a fluoride concentration of 3.51 mg/L and an electroconductivity of 456.01 μS/cm. The defluoridation experiment results showed that electroconductivity decreased dramatically within the first 30 min of the experiment, reaching a value of 339.10 μS/cm. Also, the conductivity was found to reduce up to 257.90 μS/cm at a charging time of 180 min, where the fluoride concentration was decreased from 3.51 mg/L up to 1.15 mg/L, which is below the amount of 1.5 mg/L as suggested by WHO (2019) at a charging time of 180 min and a flow rate of 10 mL/minute when 2.0 V was applied. The factors, such as charging time, flow rate, and applied potential, were found to affect the results, as shown in Fig. 12c. From this Figure, it has been observed that at low flow rates and high applied potentials, defluoridation increased. This is because at a low flow rate, the water sample had more time to complete the defluoridation process as compared to a higher flow rate, which used little time to contact the active sites of the electrodes. At higher applied potentials, the electric current created a strong electric double layer, which facilitated an increase in the strength of the electric double layer (EDL). Hence, more fluoride ions were electrosorbed onto the surface of the electrodes. The highest electrosorption efficiency of 67.24 % was obtained using WHAC-700 at a flow rate of 10 mL/min and an applied potential of 2.0 V for water sample C.

From the experiments in all water samples, it was observed that the electroconductivity of all water samples decreased during the electrosorption experiments, as shown in Fig. 13. This signified that the WHAC electrodes performed better in water defluoridation (Sufiani et al., 2023).

3.4. Reusability of the WHAC electrodes

The regeneration cycles of the WHAC electrodes were performed to evaluate their reusability for the successive cycles. This was conducted

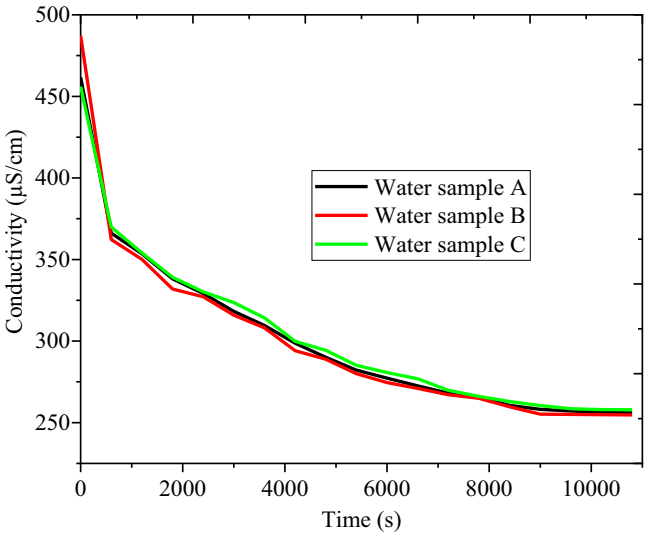

Fig. 13. Conductivity of water samples during defluoridation experiments.

over five regeneration cycles for 5 h. The results were obtained in five cycles using 3 mg/L of Fluoride (NaF) solution at 2.0 V in a charging time of 1 h and being discharged at −2 V for 30 min when the flow rate was maintained at 10 mL/min. The results showed that the desorption efficiency in the first cycle was 96.11 % and dropped to 94.01 % after 5 cycles. These results indicate that there is significant reusability of the WHAC-based electrodes similar to what Alfredy et al. (2022) reported. So, WHAC-based electrodes can be used several times during the defluoridation of water.

4. Conclusion

The porous AC has been successfully prepared from the locally available water hyacinth plants using a chemical activation method at a high activation temperature. Additionally, it has been observed that the activation temperature is crucial to the physical characteristics and electrochemical behavior of porous AC electrodes. Cyclic voltammetry was employed to assess the electrochemical properties and performance of WHAC electrodes, and their voltammograms indicated that WH plants are suitable precursors for CDI electrodes. The specific capacitance of WHAC electrodes was 354.09, 470.04, 483.73, and 501.89 F/g for CWH-400, WHAC-500, WHAC-600, and WHAC-700, respectively. The WHAC electrodes have effectively removed fluoride from water samples due to the good electrochemical properties of the synthesized electrodes, where 69.60 %, 70.28 %, and 67.24 % of fluoride was removed from water samples A, B, and C, respectively. The CDI cell used electrostatic force to remove fluoride ions from the water sample and attract them to the surface of the porous AC-based electrodes due to the electrical double layer (EDL) formed. It has been observed that the specific capacitance of the AC material is directly proportional to the specific surface area. The WHAC-700 electrode has exhibited the most significant specific surface area, pore volume, and specific capacitance. The factors that are responsible for the CDI process include specific surface area, pore volume, pore size, and specific capacitance. Hence, WHAC electrodes are suitable for water defluoridation using CDI technology. Due to high specific capacitance, the WHAC can be used in high-performance supercapacitors.

5. Limitations/recommendations of the study

The results have shown that the absence of sufficient functional groups on the electrode surface reduces efficiency; therefore, further research is needed to improve the working performance of water hyacinth-activated carbon by modifying the functional groups on the electrode surface. In addition to the nitrogen adsorption/desorption isotherm, the pore size distribution will provide a better view of the porosity of the AC. Therefore, it is recommended in further research to generate the pore size distribution curve. In this research, the reusability of the WHAC was tested for only five cycles; it is recommended that further research be conducted to test its reusability for >50 cycles. The presence of competing ions has been shown to affect water defluoridation, reducing the performance of the WHAC electrodes. Therefore, further research is also suggested to be conducted on the study of the influence of competing ions on defluoridation.

Funding statement

The authors did not receive any financial support from any organization for the submitted work.

Ethics approval

There is no need for ethical approval because this research does not involve any humans or animals.

CRediT authorship contribution statement

Hassan Johnson Kalilo: Writing – original draft, Methodology, Investigation, Conceptualization. **Joyce Elisadiki:** Writing – review & editing, Supervision, Methodology, Conceptualization. **Maheswara Rao Vegi:** Writing – review & editing, Supervision, Methodology, Conceptualization. **Said Ali Hamad Vuai:** Writing – review & editing, Supervision, Methodology, Conceptualization.

Declaration of competing interest

The authors declare that they have no known competing financial interests or personal relationships that could have appeared to influence the work reported in this paper.

Acknowledgements

The authors would like to thank the Department of Chemistry at the College of Natural and Mathematical Sciences, University of Dodoma, Dodoma, Tanzania, for providing them with the opportunity to conduct this research work.

Data availability

All the data needed for this research article was included in the manuscript.

References

Adinaveen, T., Kennedy, L.J., Vijaya, J.J., Sekaran, G., 2013. Studies on structural, morphological, electrical and electrochemical properties of activated carbon prepared from sugarcane bagasse. J. Ind. Eng. 19 (2013), 1470e1476.

Alfredy, T., Elisadiki, J., Kim, Y., Jande, Y.A.C., 2023. Water defluoridation using Al/Fe/Ti ternary metal oxide-loaded activated carbon by capacitive deionization. Environ. Sci. 9 (3), 957–972. https://doi.org/10.1039/d2ew00614f.

Alfredy, Tusekile, Elisadiki, J., Jande, Y.A.C., 2022. Capacitive deionization: a promising technology for water defluoridation: a review. Water Supply 22 (1), 110–125. https://doi.org/10.2166/ws.2021.287.

Ali, et al., 2019. Concentration of fluoride in groundwater of India: a systematic review, meta-analysis and risk assessment. Groundw. Sustain. Dev. 9, 100224. https://doi.org/10.1016/j.gsd.2019.100224.

Anton, Z., Marek, M., Slavomír, H., Michal, L., Zuzana, D., Milota, K., Jaroslav, B., 2016. Preparation of chemically activated carbon from waste biomass by single-stage and two-stage pyrolysis. J. Clean. Prod. 643–653. https://doi.org/10.1016/j.jclepro.2016.12.061.

Ayoob, S., Gupta, A.K., Bhat, V.T., 2008. A conceptual overview on sustainable technologies for the defluoridation of drinking water. Crit. Rev. Env. Sci. Technol. 38 (6), 401–470. https://doi.org/10.1080/10643380701413310.

Barbosa, R., & Pacheco, D. (2021). ScienceDirect activated carbon from water hyacinth as electrocatalyst for oxygen reduction reaction in an alkaline fuel cell. 6, 0–9. https://doi.org/10.1016/j.ijhydene.2021.04.094.

Bharath, G., Hai, A., Rambabu, K., Pazhanivel, T., Hasan, S.W., Banat, F., 2021. Designed assembly of Ni/MAX (Ti3AlC2) and porous graphene-based asymmetric electrodes for capacitive deionization of multivalent ions. Chemosphere 266, 129048. https://doi.org/10.1016/j.chemosphere.2020.129048.

Biglari, H., 2016. Geochemical study of groundwater conditions with special emphasis on fluoride concentration, Iran. Desalin. Water Treat. 57, 22392–22399. https://doi.org/10.1080/19443994.2015.1133324.

Boulika, H., El Hajam, M., Hajji Nabih, M., Idrissi Kandri, N., Zerouale, A., 2022. Activated carbon from almond shells using an eco-compatible method: screening, optimization, characterization, and adsorption performance testing. RSC Adv. 12 (53), 34393–34403. https://doi.org/10.1039/d2ra06220h.

Chen, Y., Zhu, Y., Li, Y., Wang, Z., Wang, L., Ding, L., Guo, Y., 2011. Application studies of activated carbon derived from rice husks produced by chemical-thermal process—a review. Adv. Colloid Interf. Sci. 163, 39–52.

Cho, Y., Yoo, C.Y., Lee, S.W., Yoon, H., Lee, K.S., Yang, S., Kim, D.K., 2019. Water Res. 151, 252–259, 2019.

Choi, H., Kim, D., Kim, D.G., Kim, Y., Park, J.G., Kim, M.-G., Kang, S., 2024. Improved performance of flow-electrode capacitive mixing through N-doping of activated carbon. Desalination 581, 117591.

Chowdhury, 2019. A critical review on geochemical and geological aspects of fluoride belts, fluorosis and natural materials and other sources for alternatives to fluoride exposure. J. Hydrol. 574 (2019), 333–359. https://doi.org/10.1016/j.jhydrol.2019.04.033.

Dong, Q., Yang, D., Luo, L., He, Q., Cai, F., Cheng, S., Chen, Y., 2021. Engineering porous biochar for capacitive fluorine removal. Sep. Purif. Technol. 257 (July 2020), 117932. https://doi.org/10.1016/j.seppur.2020.117932.

Dubey, S., Agarwal, M., Gupta, A.B., 2018. Recent developments in defluoridation of drinking water in India. Environmental Pollution. Springer, Berlin, Germany, pp. 345–356, 2018.
Elisadiki, J., YAC, J., RL, M., TE, K., 2019a. Porous carbon derived from artocarpus heterophyllus peels for capacitive deionization electrodes. Carbon 147, 582–593. https://doi.org/10.1016/j.carbon.2019.03.036.
Elisadiki, Joyce, Jande, Y.A.C., Kibona, T.E., & Machunda, R.L. (2019b). Highly porous biomass-based capacitive deionization electrodes for water defluoridation. https://doi.org/10.1007/s11581-019-03372-z.
Elisadiki, Joyce, Jande, Y.A.C., Machunda, R.L., Kibona, T.E., 2019c. Porous carbon derived from artocarpus heterophyllus peels for capacitive deionization electrodes. Carbon 147, 582–593. https://doi.org/10.1016/j.carbon.2019.03.036.
Elisadiki, J., Jande, Y.A.C., Kibona, T.E., Machunda, R.L., 2020. Highly porous biomass-based capacitive deionization electrodes for water defluoridation. Ionics 26 (5), 2477–2492.
Emamjomeh, M.M., Sivakumar, M., Varyani, A.S., 2011. Analysis and the understanding of fluoride removal mechanisms by an electrocoagulation/flotation (ECF) process. Desalination 275, 102–106, 2011.
Erabee, I.K., Ahsan, A., Zularisam, A.W., Idrus, S., Daud, N.N.N., Arunkumar, T., Al-Rawajfeh, A.E., 2017. A new activated carbon prepared from sago palm bark through physiochemical activated process with zinc chloride. Eng. J. 21 (5), 1–14. https://doi.org/10.4186/ej.2017.21.5.1.
Foo, K.Y., Hameed, B.H., 2009. A short review of activated carbon assisted electrosorption process: an overview, current stage and future prospects. J. Hazard. Mater. 170 (2–3), 552–559. https://doi.org/10.1016/j.jhazmat.2009.05.057.
Fritzmann, C., Löwenberg, J., Wintgens, T., Melin, T., 2007. State-of_the-art of reverse osmosis desalination. Desalination 216, 1–76. https://doi.org/10.1016/j.desal.2006.12.009.
Gaikwad, M.S., Balomajumder, C., 2017. Tea waste biomass activated carbon electrode for simultaneous removal of Cr (VI) and fluoride by capacitive deionization. Chemosphere 184, 1141–1149.
Girgis, B.S., Temerk, Y., Gadelrab, M.M., Abdullah, I.D., 2007. X-ray Diffraction Patterns of Activated Carbons Prepared under Various Conditions. Carbon Lett. 8, 95–100. https://doi.org/10.5714/CL.2007.8.2.095.
Gumus, R.H., Okpeku, I., 2015. Production of activated carbon and characterization from snail shell waste. Adv. Chem. Eng. Sci. 05 (01), 51–61. https://doi.org/10.4236/aces.2015.51006.
Huang, P.H., Jhan, J.W., Cheng, Y.M., Cheng, H.H., 2014. Effects of carbonization parameters of moso-bamboo-based porous charcoal on capturing carbon dioxide. Sci. World J. 2014 (2014), 937867.
Hui, T.S., Zaini, M.A.A., 2015. Potassium hydroxide activation of activated carbon: a commentary. Carbon Lett. 16 (2015), 275e280.
Kabir, H., 2020. Fluoride and human health: systematic appraisal of sources, exposures, metabolism, and toxicity. Crit. Rev. Env. Sci. Technol. 50, 1116–1193. https://doi.org/10.1080/10643389.2019.1647028.
Kaiwen, Z., Yuanyuan, L., Ming, Z., Xi, Y., Mengyan, Z., Ling, S., Jue, C., 2017. The porous carbon derived from water hyacinth with well-designed hierarchical structure for supercapacitors. J. Power Sources 366, 270–277. https://doi.org/10.1016/j.jpowsour.2017.09.034.
Kim, 2011. Geochemical characteristics of fluoride in groundwater of Gimcheon, Korea: lithogenic and agricultural origins environ. Earth Sci. 63 (2011), 1139–1148. https://doi.org/10.1007/s12665-010-0789-7.
Kitalika, A., Machunda, J., Revocatus, L., Komakech, H., Njau, C., Karoli, N., 2018. Fluoride variations in rivers on the slopes of mount Meru in Tanzania. J. Chem. 2018, 1–18.
Ku, Y., Chiou, H.M., 2002. The adsorption of fluoride ion from aqueous solution by activated alumina. Water Air Soil Pollut. 133, 349–361, 2002.
Kumar, 2017. Batch technique to evaluate the efficiency of different natural adsorbents for defluoridation from groundwater. App. Water Sci. 7 (2017), 2597–2606. https://doi.org/10.1007/s13201-016-0473-5.
Lacson, 2021. Fluoride containing water: a global perspective and a pursuit to sustainable water defluoridation management-an overview. J. Clean. Prod. 280, 124236. https://doi.org/10.1016/j.jclepro.2020.124236.
Lal, M.S., Sundara, R., 2022. Ceram. Int. 48, 20351–20361, 2022.
Leong, Z.Y., Yang, H.Y., 2020. Capacitive Deionization of Divalent Cations for Water Softening Using Functionalized Carbon Electrodes. ACS Omega 5 (5), 2097–2106. https://doi.org/10.1021/acsomega.9b02330.
Li, H., Zou, L., Pan, L., Sun, Z., 2010. Novel graphene-like electrodes for capacitive deionization. Env. Sci. Technol. 44 (2010), 8692e8697.
Liang, J., Tang, D., Huang, L., Chen, Y., Ren, W., Sun, J., 2018. High oxygen reduction reaction performance nitrogen-doped biochar cathode: a strategy for comprehensive utilizing nitrogen and carbon in water hyacinth. Bioresour. Technol. 267, 524e31. https://doi.org/10.1016/j.biortech.2018.07.085.
Liu, X., Liu, H., Mi, M., Kong, W., Ge, Y., Hu, J., 2019. Sep. Purif. Technol. 224, 44–50, 2019.
Matsubara, E.Y., Lala, S.M., Rosolen, J.M., 2010. Lithium storage into carbonaceous materials obtained from sugarcane bagasse. J. Braz. Chem. Soc. 21 (2010), 1877e1884.
Meenakshi, 2006. Fluoride in drinking water and its removal. J. Hazard. Mater. 137, 456–463. https://doi.org/10.1080/10643380600678112.
Mihayo, D., Vegi, M.R., Vuai, S.A., 2021. Defluoridation of Aqueous Solution Using Thermally Activated Biosorbents Prepared from Adansonia digitata Fruit Pericarp. Adsorp. Sci. Technol. 12, 1–16. https://doi.org/10.1155/2021/5574900.
Mihayo, D., Vegi, M.R., Vuai, Said Ali Hamad, 2022. Defluoridation of aqueous solution using raw and surface modified biosorbents prepared from *adansonia digitata* fruit pericarp. J. Dispers. Sci. Technol. 43 (12), 1812–1824. https://doi.org/10.1080/01932691.2021.1880925.
Mohanta, A., Mohanty, P.K., 2018. Dental fluorosis-revisited. Biomed. J. Sci. Technol. Res. 2 (1). https://doi.org/10.26717/BJSTR.2018.02.000667.
Mohanty, K., Jha, M., Meikap, B., Biswas, M., 2005. Preparation and characterization of activated carbons from Terminalia arjuna nut with zinc chloride activation for the removal of phenol from wastewater. Ind. Eng. Chem. Res. 44 (2005), 4128e4138.
Mohapatra, 2009. Review of fluoride removal from drinking water. J. Env. Manage. 91, 67–77. https://doi.org/10.1016/j.jhazmat.2006.02.024.
Mopoung, S., Moonsri, P., Palas, W., Khumpai, S., 2015. Characterization and properties of activated carbon prepared from Tamarind seeds by KOH activation for Fe(III) adsorption from aqueous solution. Sci. World J. 2015. https://doi.org/10.1155/2015/415961.
Morales, S.L., Baas-López, J.M., Romeli, B., Escobar, B., 2021. Activated carbon from Water Hyacinth as electrocatalyst for oxygen reduction reaction in an alkaline fuel cell. Int. J. Hydrogen Energy. 46 (51), 25995–26004. https://doi.org/10.1016/j.ijhydene.2021.04.094.
Nabais, J.M.V., Laginhas, C.E.C., Carrott, P.J.M., Ribeiro Carrott, M.M.L., 2011. Production of activated carbons from almond shell. Fuel Process. Technol. 92 (2), 234–240. https://doi.org/10.1016/j.fuproc.2010.03.024.
Noked, M., Avraham, E., Soffer, A., Aurbach, D., 2009. The rate-determining step of electroadsorption processes into nanoporous carbon electrodes related to water desalination. Phys. Chem. C 113 (2009), 21319e21327.
Otowa, T., Tanibata, R., Itoh, M., 1993. Production and adsorption characteristics of MAXSORB: high-surface-area active carbon. Gas Sep. Purif. 7 (1993), 241e245.
Porada, S., Zhao, R., van der Wal, A., Presser, S., PM, B., 2013. Review on the science and technology of water desalination by capacitive deionization. Prog. Mater. Sci. 58, 1388–1442. https://doi.org/10.1016/j.pmatsci.2013.03.005.
Prahas, D., Kartika, Y., Indraswati, N., Ismadji, S., 2008. Activated carbon from jackfruit peel waste by H3PO4 chemical activation: pore structure and surface chemistry characterization. Chem. Eng. J. 140 (2008), 32e42.
Qina, M., Deshmukha, A., Epszteina, R., Patela, S.K., Owoseni, O.M., Walker, W.S., Elimelecha, M., 2019. Comparison of energy consumption in desalination by capacitive deionization and reverse osmosis. Desalination 455 (November 2018), 100–114. https://doi.org/10.1016/j.desal.2019.01.003.
Quach, N.K.N., W-D, Y., Z-J, C., HL, T., 2017. The influence of the activation temperature on the structural properties of the activated carbon xerogels and their electrochemical performance. Adv. Mater. Sci. Eng. 2017, 1–9. https://doi.org/10.1155/2017/8308612.
Rambabu, K., Bharath, G., Hai, A., Luo, S., Liao, K., Haija, M.A., Naushad, M., 2020. Development of watermelon rind derived activated carbon/manganese ferrite nanocomposite for cleaner desalination by capacitive deionization. J. Clean. Prod. 272, 122626. https://doi.org/10.1016/j.jclepro.2020.122626.
Rangari, P.J., Chavan, P., 2017. A review on preparation of acti_vated carbon from coconut shell. Int. J. Innov. Res. Sci. Eng. Technol. 6 (4), 5829–5849, 2017.
Saldaña-robles, A., Arcibar-orozco, J.A., Guerrero-mosqueda, L.R., Damián-ascencio, C. E., Marquez-herrera, A., Corona, M., … Cano-andrade, S. 2023. (2023). Synthesis of composites for the removal of F − anions. 1–22.
Sharma, A., Aggarwal, N.K., 2020. Water Hyacinth: A Potential Lignocellulosic Biomass for Bioethanol. Springer, Cham. https://doi.org/10.1007/978-3-030-35632-3.
Singh, et al., 2017. Adsorption of fluoride from industrial wastewater in fixed bed column using Java plum (syzygium Cumini). Asian J. Pharm. Clin. Res. 9, 320. https://doi.org/10.22159/ajpcr.2016.v9s3.12613.
Stephanie, H., Mlsna, T.E., Wipf, D.O., 2021. Functionalized biochar electrodes for asymmetrical capacitive deionization. Desalination 516, 115240.
Sufiani, O., Elisadiki, J., Tanaka, H., Teshima, K., Sahini, M.G., Machunda, R.L., Jande, Y. A., 2023. Adsorption-capacitive deionization hybrid system with activated carbon of modified potential of zero charge. Environ. Res. 219, 115114.
Sun, K., Wang, Y., Zhang, L., Shao, Y., Li, C., Zhang, S., Hu, X., 2024. High yield of carbonaceous material from biomass via. Chem. Eng. J. 485 (February), 149823. https://doi.org/10.1016/j.cej.2024.149823.
Tang, W., Kovalsky, P., Cao, B., He, D., Waite, T.D., 2026. Fluoride Removal from Brackish Groundwaters by Constant Current Capacitive Deionization (CDI). Environ. Sci. Technol. 50 (19), 10570–10579. https://doi.org/10.1021/acs.est.6b03307.
Waghmare, S.S., Arfin, T., 2015. Fluoride removal from water by various techniques. Int. J. Innov. Sci. Eng. Technol. 2 (3), 560–571.
Wang, J., Kaskel, S., 2012. KOH activation of carbon-based materials for energy storage. J. Mater. Chem. 22 (2012), 23710.
Who. (2011). Guidelines for drinking-water quality, 4th ed., vol. 38. WHO chronicle, pp. 104–108. (4). 4.
WHO, 2003. Shaping the Future, 2003. World Health Organization, Geneva, Switzerland.
WHO, 2019. Inadequate or excess flouride: a major public health concern. Retrieved from. https://www.who.int/teams/environment-climate-change-and-health/chemical-safety-and-health/inadequate-or-excess-fluoride.
Wu, K., Gao, B., Su, J., Peng, X., Zhang, X., Fu, J., Chu, P.K., 2016. RSC advances hyacinth for high-performance supercapacitors. RSC Adv. 6, 29996–30003. https://doi.org/10.1039/C5RA25098F.
Yang, J., Zhang, Z., Madabattula, G., Wu, B., Performance, D., Ntakirutimana, S., … Marc, A. (2020). The physical and electrochemical properties of activated carbon electrode derived from pineapple leaf waste for supercapacitor applications. https://doi.org/10.1088/1742-6596/1655/1/012008.
Yasin, A.S., Mohamed, I.M.A., Mousa, H.M., Park, C.H., Kim, C.S., 2018. Facile synthesis of TiO2/ZrO2 nanofibers/nitrogen co-doped activated carbon to enhance the desalination and bacterial inactivation via capacitive deionization. Sci. Rep. 8 (2018), 541.
Yeh, C.L., Hsi, H.C., Li, K.C., & Hou, C.H. (2015). Desalination 2015, 367, 60–68.

Zhan, Y., Zhou, H., Guo, F., Tian, B., Du, S., Dong, Y., Qian, L., 2021. Preparation of highly porous activated carbons from peanut shells as low-cost electrode materials for supercapacitors. J. Energy Storage 34, 102180.

Zhang, et al., 2018. Three-dimensional honeycomb-like porous carbon derived from corncob for the removal of heavy metals from water by capacitive deionization. RSC Adv. 8, 1159–1167. https://doi.org/10.1039/c7ra10689k.

Zhang, M., Kong, W.J., 2020. Electroanal. Chem. 878, 114703, 2020.

Zhao, et al., 2017. Removal of NaCl from saltwater solutions using micro/mesoporous carbon sheets derived from watermelon peel via deionization capacitors. RSC Adv. 7, 4297–4305. https://doi.org/10.1039/c6ra27127h.Journal.

Zhou, Z., Yu, Y., Ding, Z., Zuo, M., Jing, C., 2019. Competitive adsorption of arsenic and fluoride on {201} TiO2. Appl. Surf. Sci. 466, 425–432, 2019.

Zornitta, R.L., García-Mateos, F.J., Lado, J.J., Rodríguez-Mirasol, J., Cordero, Hammer, T.P., Ruotolo, L.A.M, 2017. High-performance activated carbon from poly_aniline for capacitive deionization. Carbon 123 (2017), 318e333.